Simulating the signal of a scintillator hodoscope

F. A. Sánchez*, G. Medina-Tanco*

Instituto de Ciencias Nucleares, Universidad Nacional Autónoma de México, México, D.F., C.P. 04510.

***Abstract*. Muons, photons, electrons and positrons are the most abundant secondaries of cosmic rays at ground level. While muons penetrate deeply in almost straight paths, highly energetic γ and $e^{\pm}$ develop small underground showers which are stopped in first few meters. This difference may be used to distinguish footprints on buried detectors with x-y sensitivity. In this work we present fast and robust simulations techniques to emulate realistically the response of a scintillator based hodoscope. Processes such as energy deposition, photon yield, transport of light in plastic scintillators and optical fibers, as well as electronic PMT signal formation are taken into account. All free parameters in our simulations were calibrated using laboratory measurements.**

***Keywords*: Detector simulation, Hodoscope, Instrumentation**

I. Introduction

Among others, the scintillator based detectors are between the most commonly used in cosmic ray and particle physics. Applied either as a counters, veto-setters or even tracking hodoscopes [1], [2], [3], [4] are widely used in the high energy field. The scope of the work we are presenting here is to provide a fast and robust simulation technique to emulate realistically the response of detectors based on scintillator strips embedded with wavelength shifter fibers (WLS) and coupled to fast photomultipler tubes (PMT). This basic device unit is on the roots of many, and more complex, detectors. In this sense, our code can very easily be extended to a large variety of experiments and, in particular, to cosmic ray hodoscopes [5], [6].

II. Simulation technique

The aim of the simulation package we are presenting here is to convert the energy deposited in a scintillator strip, E_{dep}, to a PMT voltage signal $V(t)$ taking into account the photon yield in the plastic scintillator, the transport and reflection of light in the strip and the absorption and emission of photons in the WLS. Several variables determine the actual signal generation, however the expected light yield can be estimated by means of generals arguments.

It is known that typical energy gaps between molecular excited states of the scintillator plastic are $\sim$ 4-5 eV. Assuming that around 5% of the energy is converted to fluorescence photons, then $\sim \frac{4\text{ eV}}{5\%} = 80$ eV are needed to produce one single scintillation blue photon (or $Y \sim 1.25 \times 10^4$photons/MeV). Before reaching the PMT's photo-cathode, the produced photons must be absorbed and re-emitted as a green photons within the proper acceptance cone of the WLS fiber. They must, therefore, survive the bulk and wall absorption in the plastic. The probability for a blue photon to be absorbed by the WLS can be estimated as [7] $p_W = \frac{d_f/w_s}{(1-e^{-w_s/\lambda})+(1-R)+d_f/w_s}$ where d_f is the fiber diameter, w_s is the strip width, λ is the scintillator attenuation length and R is the reflection coefficient of the walls. On the other hand, the transmission probability for meridional photons inside the WLS fiber is determined by $p_T = \frac{1}{2}(1 - n_{clad}/n_{core})$, where n_{clad} and n_{core} are the refractive index of the core and cladding respectively (typical values for this to variables are n_{core}=1.6 and n_{clad}=1.49).

If the attenuation along the fibre is $A_{tt}(x)$, then a charged particle traversing the scintillator strip at a distance x from the PMT will produce

$$E_{dep} \times \underbrace{Y \times p_w \times p_T}_{k} \times A_{tt}(x) \qquad (1)$$

photons. For a device with d_f=1.5mm, w_s=4cm,λ=10cm and R=98%, k results $\approx$ 33 photons/MeV. Only a fraction of these photons will be capable to pull an electron out of the cathode. Assuming a quantum efficiency $p_Q \sim$10% we expect $k \times p_Q \approx 3.3$ photo-electrons/MeV. In our simulation, the product $k_Q = k \times p_Q$ (i.e., the number of photo-electrons per energy unit at the deposition point) is a free parameter that must be tuned

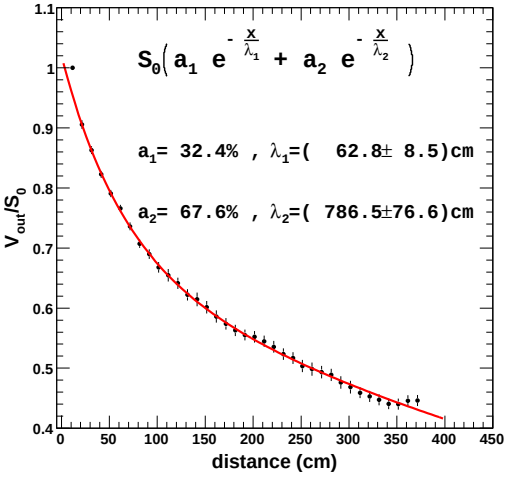

Fig. 1. Exponential behaviour of the light attenuation in WLS fibers, $A_{tt}(x)$. The typical double decay law is clearly appreciable.

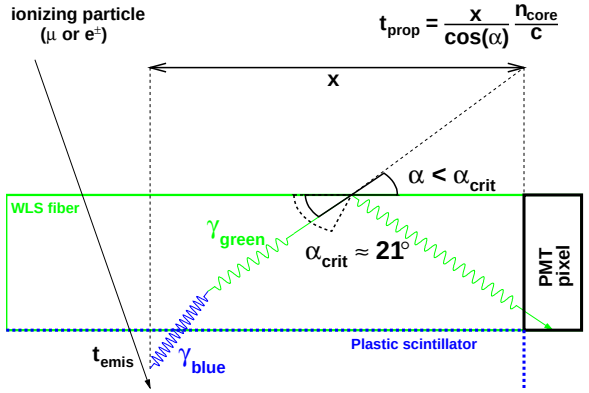

Fig. 2. Timing simulation scheme for a WLS photon radiated, with an angle α, at the instant t_{emis} from a distance x.

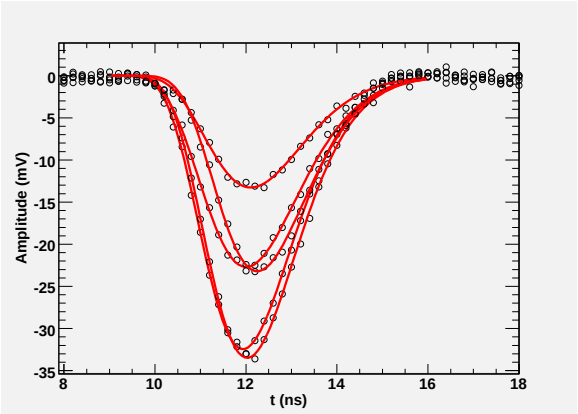

Fig. 3. Some measured single-photoelectron pulses and their fit. The fitting function,$V_i^{phe}(t)$, is defined in (4). For each measured pulse, the fitting parameters are V_i^{max} and τ_i

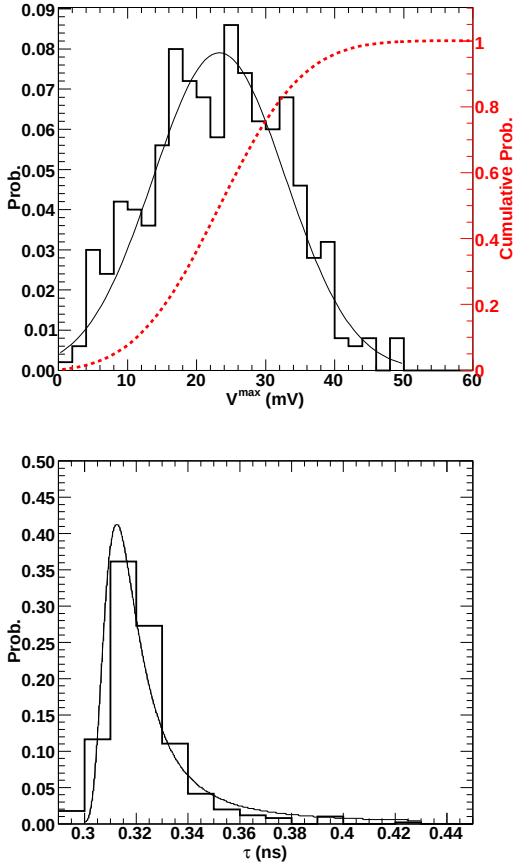

Fig. 4. Experimental τ_i (bottom) and V_i^{max} (top) with the parametrized fit distributions used in the simulation.

to match the measurements. We found that k_Q^{Sim} = 3phe/MeV (see next section) reproduces very accurately the observations and is in good agreement with the expected value.

The light attenuation along the fiber was carefully measured and characterized in the laboratory. The light intensity as a function of distance decreases with a double exponential decay law which is shown in Fig.1. As can be seen, almost 30% of the light is absorbed in the first 60cm of the WLS fiber.

Any signal $V(t)$ generated by a PMT will be a superposition of single photo-electron pulses $V_i^{phe}(t_i)$. The times t_i depend mainly on the time of emission of the scintillation photons t_{emis}, on the delay due to propagation in the fiber t_{prop}, and, finally, on the transit time spread of the PMT, t_{TT}. The emission times [8] follow the distribution

$$1/(1+R)(\frac{e^{-t/\tau_2}-e^{-t/\tau_1}}{\tau_2-\tau_1}+\frac{R}{\tau_3}e^{-t/\tau_3}) \qquad (2)$$

where τ_1=0.5ns and τ_2=1ns are two fast decay constants while τ_3=6ns is the slow decay time constant. The fraction of slow to fast component is R=5.

The propagation delays are $t_{prop} = \frac{x}{\cos\alpha} \times \frac{n_{core}}{c}$ (see Fig.2) where α, the emission angle inside the fiber, is isotropically distributed. The transit times are randomly chosen from a Gaussian distribution with mean 12ns and sigma 1.85ns.

The overall PMT output signal is constructed by summing the contributions of indivual photo-electrons

$$V(t) = \sum_{i=1}^{N_{phe}} V_i^{phe}(t-t_i) \qquad (3)$$

where $t_i = t_{emis} + t_{prop} + t_{TT}$ and $P(N_{phe}|n_{phe})$ is the poisson probability of having N_{phe} photo-electrons if the expected mean is $n_{phe} = E_{dep} \times k_Q \times A_{tt}(x)$.

The response function of a single photo-electron pulse is

$$V_i^{phe}(t) = \frac{V_i^{max}}{n^n e^{-n}} \left(\frac{t}{\tau_i}\right)^n e^{-t/\tau_i} \qquad (4)$$

with $n = 10$. In order to reproduce accurately the signal-to-signal fluctuations, for every photo-electron participating in (3), the parameters V_i^{max} and τ_i are randomly chosen from previously measured distributions. In Fig.3 are shown some fits to real single photo-electron pulses using (4) as a fitting function. The resulted distributions of V_i^{max} and τ_i for a 10,000 fits are shown in Fig.4. It is worth to note that the measured probability of having a single photo-electron pulse of amplitude greater

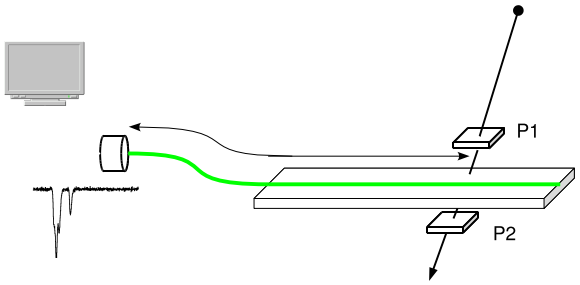

Fig. 5. Experimental setup to record real muon signal at a given X distance from the PMT. A coincidence between detectors P1 and P2 triggers the data acquisition. The recorded pulses were used to tune simulation free parameters k_Q, R and τ_3.

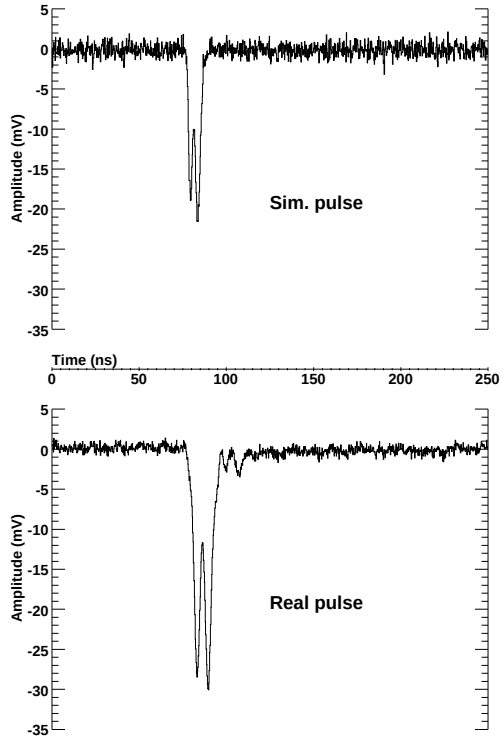

Fig. 6. A real (bottom) and a simulated (top) muon pulse example. These signals should not be compare except in their general features as can be the time structure and pulse height.

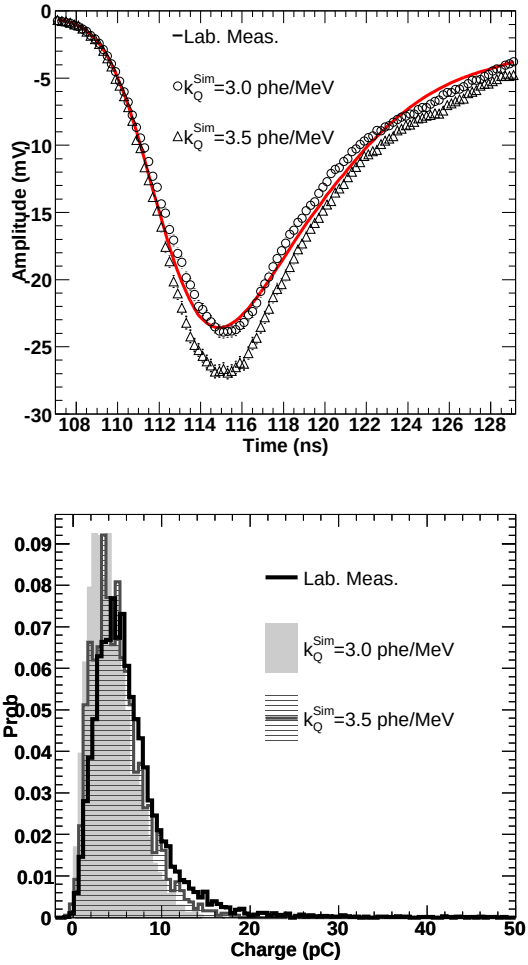

Fig. 7. Parameters calibration example: mean pulse (top) and charge distribution (bottom) for k_Q^{Sim}=3 and 3.5phe/MeV.

than 20mV is ≈70% (see the dashed line in the Fig.4). In other words, if a discrimination threshold is set to 20mV, the probability of triggering with electronic dark pulses is 70%. Although this may seem a relatively high probability, phototubes commonly used in modern physics experiments have dark rates of very low frequency. Generally dark pulses occur at ∼5-15Hz and do not interfere with most of desidered observables.

The electronic white noise was also measured and properly added to the resulting simulated signals.

III. Calibration of free parameters

The energy deposition in a strip was calculated by means of the GEANT4 package [9]. The input to start the simulation chain were muons with their momenta spectrum coming from

$$I(p_\mu, \theta) = \cos^3(\theta) I_v(p_\mu \cos(\theta)) \quad (5)$$

to fairly reproduce the observed distribution at ground level [10]. For each event, the corresponding ligth yield, photon transmission and attenuation were calculated following the rationale described in the previous section. Finally the electronic PMT response were build usign formula (3).

As above mentioned, the free parameters of the simulation code (i.e., k_Q, R and τ_3) were calibrated using actual muon signals. To this aim, we recorded 10,000 pulses produced by background muons as schematically shown in Fig.5. The statistical features of real signals were compared with those coming out from the simulation and the free parameter adjust until a good agreement was achieved. Fig.6 shows a random example of a real and a simulated signal (beware: those signals should not be compare with each other except in their general features because do not have the same event's conditions). More relevant to the parameter

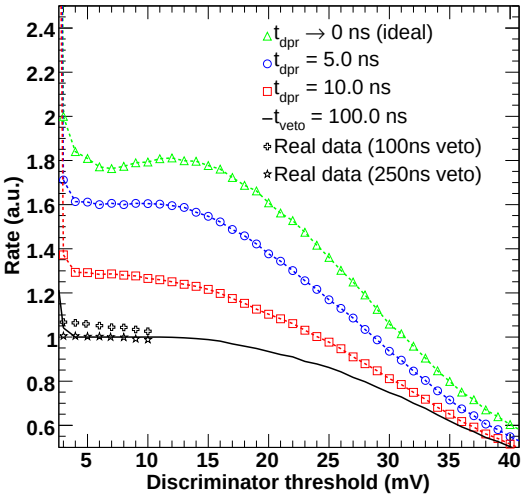

Fig. 8. The effects of the discriminator double peak resoluton time, t_{dpr}, on the counting rates of background atmospheric muons. The solid line is the prediction based on our simulations if a veto of 100 ns is applied. Star and cross markers are real data.

calibration are the statistics comparison. As an example, the mean pulse and the charge distribution for k_Q^{Sim}=3 and 3.5phe/MeV are shown in Fig.7. As mentioned in the previous section, k_Q^{Sim}=3phe/MeV fit better to the measured data. Even if the charge distributions are very similar to each other, the real distribution shows a longer tail which is produced by an undershoot present in the real signals -appreciable in Fig.6- and not yet implemented in our simulations.

IV. A SIMPLE APPLICATION: STRIP EFFICIENCY TO ATMOSPHERIC BACKGROUND MUONS

The thorough study of the response of a scintillator hodoscope of complex geometry, is beyond the scope of this work. Nevertheless, as a simple example, we report on the efficiency of a single scintillator strip (the basic unit of such kind of detectors) used as a muon counter.

We assume a scenario routinely used in a large variety of experiments consisting in a PMT attached to a front-end electronic board which discriminates and digitizes the input signals. One important characteristic of discriminators, that must be taken into account during the design phase of any experimental device, is specified in terms of their double peak resolution time, t_{dpr}. This time is defined as the time between the leading edges of the two most closely spaced input pulses for which the discriminator produce two output pulses. Typical values for t_{dpr} are 5-10 ns in modern discriminators. Because the time structure present in the muon pulses (as the double peak shown in Fig.6) an ideal discriminator ($t_{dpr} \rightarrow 0$) with its threshold set to a low value will resolve the multiple peaks of the signals leading to an overcounting of individual muons. On the other hand, if the threshold is too high, many signals will be rejected resulting in a misleadingly low counting rate. We show in Fig.8 the effects of differents t_{dpr} on the counting rates. As can be seen, an ideal discriminator would count almost 80% more muons or, putting the same in other words, would count practically 2 peaks per muon signal. Realistic values of t_{dpr} do not solve the problem completely. One way to avoid the overcounting is to inhibit the second or subsequent peaks by means of a veto time window, t_{veto}. In this manner, input pulses are ignored during the time the inhibit veto is applied. The best value for t_{veto} will depend on the details of detector being design and on the physics observables to be measured. In our toy example of a counting strip for atmospheric background muons, we show that a t_{veto} around 100ns should be enough to eliminate the overcounting for thresholds in the range $\approx$2-20mV. Nevertheless, when this condition is applied to real data, we see that a higher veto is needed (see Fig.8). A possible explanation could come from reflected pulses at the farthest edge of the real strip which was white painted. Such reflections could increase the peak multiplicity at longer times and were not consider in the simulations.

V. CONCLUSIONS

We have report on a robust and fast simulation code to reproduce realistically the response of generic scintillator strips of the kind widely used in particle and cosmic ray physic experiments. The implemented code starts with the energy deposition of charged particles and ends with electronic signals produce by a standard PMT. All the free parameters of the simulation were tuned with laboratory measurement. This ansatz it is flexible enough to implement the code to different experimental devices based on plastic scintillation techniques of the kind presented here. Furthermore, our code can be coupled with extended air shower simulation packages [11] to assess the response of multilayer scintillator based hodoscopes and perform shielding studies.

ACKNOWLEDGEMENTS

This work is supported by CONACyT (Mexico). Authors also acknowledge financial aid from UNAM through CIC and DGAPA-PAPIIT grants.

REFERENCES

[1] F. Carminati *et al.*, J. Phys. G **30** (2004) 1517.
[2] B. Cheynis *et al.*, Nucl. Instrum. Meth. A **569** (2006) 732.
[3] A. Fernandez *et al.*, International Conference: New Trends in High-Energy Physics, Crimea, 2006, arXiv:physics/0612051v1
[4] A. Etchegoyen, 30th International Cosmic Ray Conference 2008, Vol. 5, pages 1191
[5] F. Sanchez *et al.*, 30th International Cosmic Ray Conference 2008, Vol. 5, pages 1175,
[6] F. Sanchez *et al.*, 30th International Cosmic Ray Conference 2008, Vol. 5, pages 1179,
[7] C.P Achenbach, arXiv:nucl-ex/0404008v1.
[8] J.W. Nam, Nucl. Instrum. Meth. A **491** (2002).
[9] S. Agostinelli *et al.*, Nucl. Instrum. Meth. A **506** (2003). http://geant4.web.cern.ch/geant4
[10] D. Reyna, arXiv:hep-ph/0604145.
[11] S. Sciutto, http://www.fisica.unlp.edu.ar/auger/aires/